



HAL
open science

Methodology to assess interlayer quality in the material extrusion process: a temperature and adhesion prediction on a high performance polymer

Arthur Lepoivre, Nicolas Boyard, Arthur Lévy, Vincent Sobotka

► To cite this version:

Arthur Lepoivre, Nicolas Boyard, Arthur Lévy, Vincent Sobotka. Methodology to assess interlayer quality in the material extrusion process: a temperature and adhesion prediction on a high performance polymer. Additive Manufacturing, 2022, 60, pp.103167. 10.1016/j.addma.2022.103167 . hal-03806235

HAL Id: hal-03806235

<https://hal.science/hal-03806235>

Submitted on 7 Oct 2022

HAL is a multi-disciplinary open access archive for the deposit and dissemination of scientific research documents, whether they are published or not. The documents may come from teaching and research institutions in France or abroad, or from public or private research centers.

L'archive ouverte pluridisciplinaire **HAL**, est destinée au dépôt et à la diffusion de documents scientifiques de niveau recherche, publiés ou non, émanant des établissements d'enseignement et de recherche français ou étrangers, des laboratoires publics ou privés.

Methodology to assess interlayer quality in the material extrusion process: a temperature and adhesion prediction on a high performance polymer

Arthur Lepoivre¹, Nicolas Boyard¹, Arthur Levy¹, Vincent Sobotka^{1*}

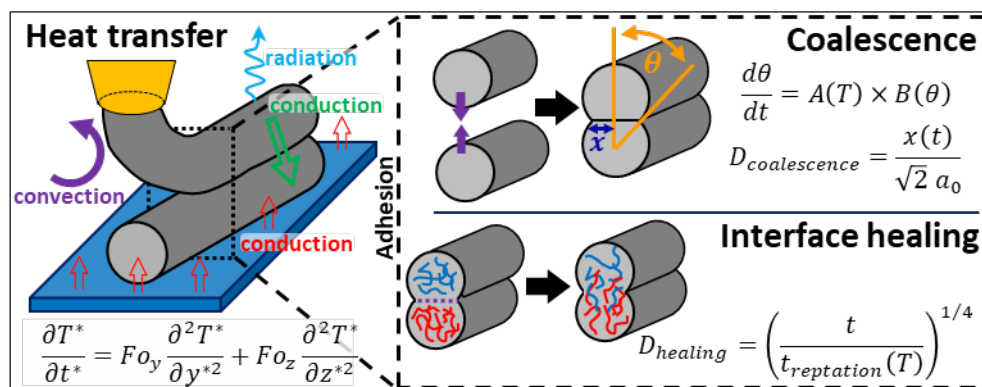
¹ Nantes Université, IRT Jules Verne, CNRS, Laboratoire de thermique et énergie de Nantes, LTeN, UMR 6607, F-44000 Nantes, France

* Corresponding author: vincent.sobotka@univ-nantes.fr

Abstract

The material extrusion additive manufacturing process consists in extruding a molten polymer along a path with trajectories defined from a 3D definition of the part. One of the major drawbacks of this process is the reduction of the mechanical properties of the parts compared with those made by conventional manufacturing methods such as injection molding. On the one hand, this reduction of properties is linked to the presence of macroporosities in the part and, on the other hand, to the limited adhesion between the deposited layers. These two phenomena strongly depend on the thermal history of the polymer. This work proposes to determine the thermal conditions leading to sufficient adhesion, and to the manufacture of parts with sufficient final interfilament strength. An instrumented bench was developed from a 3D printer in order to investigate the cooling, at the filament scale, of parts printed in PEKK material. In parallel, heat transfers in the material extrusion process were simulated using a model, which was validated with the experimental data obtained using the bench. The adhesion was also modeled by describing the phenomena of coalescence and healing of the interface. The physical properties necessary for the models were characterized taking into consideration their thermodependency. A parametric study then quantifies the influence of each parameter on the temperature of the polymer, as well as on the interlayer adhesion, thus contributing to the definition of the process window.

Graphical abstract



Keywords: Fused filament fabrication (FFF), Heat transfer, Coalescence, Interface Healing, PEKK.

1. Introduction

Additive manufacturing (AM) makes it possible to create parts by the successive addition of layers, as defined in ISO/ASTM 52900 [1]. It can be used for different applications in various industries, such as prototyping, automotive, aeronautics, aerospace, biomedical, luxury, and building. The Wohler report, the reference document

on additive manufacturing economics, stated in 2019 that additive manufacturing represented \$15.8 billion for products and services worldwide and that this should increase to \$35.6 billion in 2024 [2]. Among all AM processes, fused filament fabrication (FFF) is one of the most user-friendly, with low price machines and various materials available [3].

Today, the greatest limitations of the FFF process are the difficulties of print large parts, the long printing time, and the low mechanical resistance of the part created. Our work is specifically about this last limitation. The poor mechanical properties of the printed parts are linked: (i) to the presence of porosities between the filaments forming the part, and (ii) to the weak resistance at the interface of the successive layer stack. Indeed, the geometry of the section of the filament evolves during deposition, with an increase of the interface length versus time, as presented in Figure 1 (a), corresponding to the coalescence process. Also, the limited mechanical resistance between the filaments is due to a non-optimal healing of the interface. This interface healing takes place by the interdiffusion of the macromolecular chains of the polymer across the interface, as illustrated in Figure 1 (b). After a sufficiently long time at high temperature, the interpenetration of the chains at the interface is fully realized, leading to complete healing. The interface will then have the mechanical properties of the bulk material [4]. The coalescence process is partly driven by the evolution of the viscosity and surface tension of the material, whereas the interface healing is driven by the reptation time. These three thermophysical properties, strongly influenced by the temperature evolution, are key elements that need to be determined to accurately model adhesion.

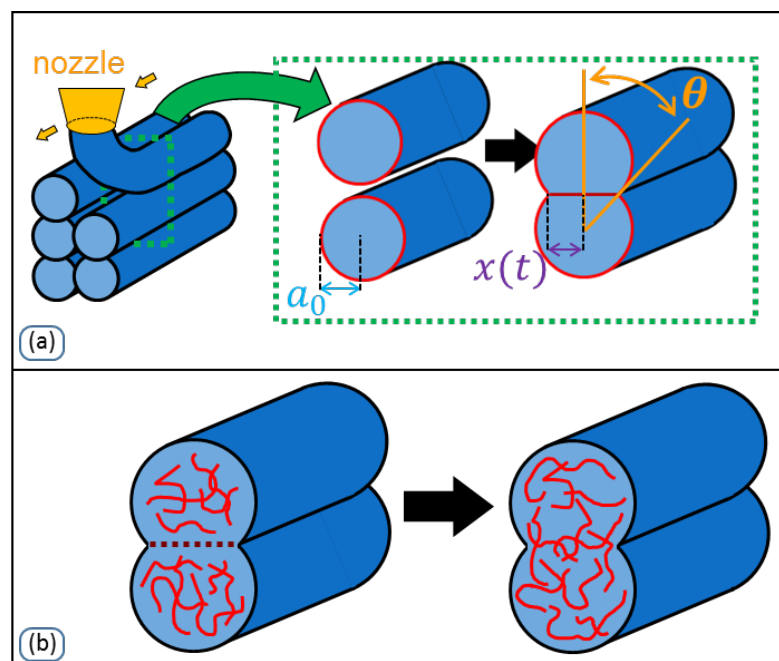


Figure 1 – Illustration of adhesion in the FFF process: (a) the coalescence process and (b) the diffusion process.

Recently, the FFF process has been considered a candidate to manufacture complex geometry parts for the aeronautic sector. This industrial application requires high performance materials to ensure appropriate specific mechanical performances. Manufacturing such high-performance materials with FFF requires specific machines. To reach high processing temperatures, the extruder should heat over 350°C. A high temperature heating chamber and plate (over 120°C) is also essential. PAEK family materials such as PEEK and PEKK are good candidates for aeronautical grade thermoplastic matrix composites. Recent development shows the interest for PEKK instead of

PEEK for the FFF process [5] because of its better layer adhesion, lower print temperature, reduced warping, fast print speeds and the advantage of being able to control the crystalline state of the material. Also, the user must pay attention to the possible degradation of this generation of polymers, which takes place at temperatures close to those used in their processing [6].

Heat transfer modelling of the FFF process has been widely discussed in the literature. The first models described the cooling of the polymer extruded using a simplified approach, with a lumped-capacity model on a 1D geometry description [7–10]. Considering a small Biot number ($Bi < 0.1$), those models proposed an analytical solution to predict the temperature of deposition of a single filament cooled only by convection. They did not describe the influence of the deposition of the other filaments needed to model the successive deposition of the layers. Additionally, they never took into account the temperature dependency of the thermal properties. Later, a 2D model [11] was proposed, describing the temperature difference between the core and the interface of the filaments, but remained limited by the ideal geometrical assumption. All these models were compared and found to differ greatly, in a study that also provided the first experimental data using a thermocouple between the support plate and the first filament [12]. More recently, Costa *et al.* [13–15] modelled the progressive addition of matter and described with more precision the contacts between filaments, the convection and radiation in the air gaps between filaments, and with the surrounding environment. However, their model remains limited by the same assumption of small Biot number. Their model was validated experimentally with an IR camera positioned above the printing area, and thus measuring the last filament deposited. Although their experimental set-up could not confirm it, they mentioned a conduction effect from the newly extruded filament influencing the temperature of the previous deposited filaments, which was later confirmed by another study [16]. More recent models are much more realistic [17–19, 60] as they consider the successive deposition pattern and describe the thermal phenomena better by including conduction with neighboring filaments with thermal contact resistances, exothermic crystallization, convection with the environment and radiation losses. In this article, we follow the modelling approach initiated in a previous work [48]. Finite elements are used and consider potential thermal heterogeneity in the filament section, thus without the small Biot number assumption. In addition to the previous work [48], thermodependent thermal properties are also characterized and implemented. Our model will be solved with a numerical tool and will consider the preponderant heat transfer phenomena to maintain computation costs at a reasonable level.

In-situ experimental temperature measurement is usually required to validate proposed models. In the literature, the experimental measurements of the filament cooling printed with the FFF process are generally divided into two categories: measurement with thermocouples [12,19–21] or with an IR camera [17,22–26]. Measurements with thermocouples remain highly intrusive and are usually done with a pause during printing. Although the IR gives the complete thermal cartography, it requires the target to be directly visible by the camera, a high spatial resolution, and knowledge of the material's radiative properties. The reported studies using an IR camera were only done at the macroscopic part scale. To describe the thermal phenomena at the filament scale with precision, we will use an infra-red measurement with a spatial resolution of 30 microns per pixels. The setup was presented in our previous work [48] where a filament thickness spans over 13 pixels. In the present paper, the measurement procedure was calibrated and validated. Our work focuses on high performance polymers, thus requiring the adaptation of the experimental bench initially developed in [48], with a heating chamber, support plate, and an extruder adapted to the high processing temperatures of PEKK materials.

Heat transfer between filaments, especially at the interfaces, can subsequently be used to predict the quality of adhesion. Interfilament adhesion in the FFF process is classically modelled with both a coalescence and a healing model. The first is classically based on Frenkel-Eshelby's description [27–29] of two spheres in coalescence and, even if the considered filaments are not spheres, it has been widely used for the FFF process [10,12,30–33]. The latter is based on the reptation theory from De Gennes [37], mainly used to describe macromolecular mobility to form a bond at the interface in thermoplastic polymers.

In order to use the coalescence and interface healing models, the interface temperature between the extruded filaments is required. This information is difficult to obtain experimentally with a non-intrusive tool. To solve this problem, we developed a numerical model of heat transfer in the FFF process using COMSOL Multiphysics® FEM software. This model requires the thermal properties density, specific heat and thermal conductivity, which were characterized. The simulation results also had to be validated with experiments, which were done on the instrumented bench designed to measure the temperature evolution of a high performance polymer at the filament scale using an IR camera. Then, in order to use the coalescence and interface healing models, the viscosity, surface tension and relaxation time were also characterized.

The three models, predicting the heat transfer, coalescence and interface healing, were then used to improve understanding of the adhesion and contribute to the definition of the process window for the FFF process with a parametric study.

2. Material and methods

2.1. Materials

The material of interest in this study is the high-performance polymer PEKK KEPSTAN™ 6004, supplied by ARKEMA®. The ratio of terephthalate/isophthalate isomers is 60/40 [38], inducing a very low crystallization kinetics [6,39] relative to the FFF process duration. Thus, hereunder, the polymer is considered in its amorphous state.

2.2. Methods for characterizing the physical properties of PEKK

2.2.1. Thermal properties

The thermal properties of PEKK KEPSTAN™ 6004 in the amorphous state were characterized with different apparatuses. The temperature dependence on the density, thermal conductivity and specific heat was considered.

The density was characterized in the glassy state with a DIL L75 PT horizontal dilatometer from LINSEIS®. In the rubbery state, a PVT-XT device [40] was used. This is a laboratory-built temperature and pressure-controlled cavity classically used for thermomechanical characterization of thermoplastics. For both methods, the geometry of the samples was a cylinder of 8 mm diameter and 12 mm height. The procedure with a dilatometer remains standard and two samples were tested. For the PVT-XT, a total of six samples were tested with five compaction pressures varying between 15 and 100 MPa. For all these measurements, the repeatability was verified by an experiment at 20 MPa on two different samples. A classic Tait model [41–44] was used to extrapolate the density to atmospheric pressure. The six coefficients of this Tait model make it possible to decouple the effects of pressure and temperature on the evolution of the density.

The specific heat was determined with a DSC Q200 from TA Instruments® on polymer samples of 5–10 mg, with a 5 K/min heating ramp. Specific heat was determined from 40 to 130°C for the glassy state and from 340 to 380°C for the rubbery state.

The thermal conductivity was determined using a hot guarded plate, at 60, 100, and 140°C. Exceptionally for this characterization and because of sampling issues, the material tested was PEKK KEPSTAN™ 6002 samples of 25 mm diameter by 4 mm thickness, cut from an injected plate of 100 x 100 x 4 mm produced by ARKEMA®. The conductivity of PEKK 6002 was assumed to be equal to that of PEKK 6004 because of the very similar nature of these polymers. Only the molecular mass of the polymer differs between these two grades.

2.2.2. Rheological properties and surface tension

The surface tension and Newtonian viscosity were also characterized. Surface tension was determined with a DSA100 tensiometer from KRÜSS®, on the temperature range from 25°C to 373°C. Newtonian viscosity was determined on a Thermo Scientific HAAKE MARS III rheometer from Thermo Fisher® on five temperatures from 340 to 380°C [45].

The relaxation time of the polymer was also determined with the same rheometer and the same temperature range of 340–380°C. The longest relaxation times were too low to be determined by a standard frequency sweep on the working range of the apparatus. In these cases, the time was determined with a creep-recovery experiment, making it possible to attain lower solicitation frequencies. A detailed description of the methodology is available in [45, 59].

2.3. Experimental approach

2.3.1. 3D-printer bench design

A novel experimental bench was specifically designed, developed, and used to study heat transfer in the FFF process with the high performance polymer [48]. The objective of this bench was to measure the thermal history of the polymer at the filament scale and during fabrication of a 3D printed part.

The printer on the bench was based on the commercial printer CR10-5S from Creality 3D®, originally designed for PLA and ABS. We adapted this machine to print high performance polymers such as PEKK. This polymer requires high transformation temperatures meaning that the commercial printer had to be modified, with a high temperature extruder, heating plate and heating enclosure, to reach higher temperatures than those usually used. The main issue was the implementation of the heating chamber, with a maximum temperature of 200°C, which must keep the air around the polymer deposition insulated from the ambient environment while allowing movement of the nozzle and plate. Also, all the electronics components had to be moved out of the chamber, because of their thermal sensitivity above 70°C.

To adapt to these technical constraints, the extruder, manufactured by TOBECA®, is completely made of metal, with closed circuit water cooling, capable of reaching the temperatures over 400°C required to print with PEKK. The heating plate is made of six heating patches fixed on a brass plate, with an electrical power of 150 W for each, regulated by an external PID and power regulator, to reach a maximum of 250°C. The heating chamber is made of two parts: a fixed structure, with a mobile part sliding vertically inside (axis Z in Figure 2). It is made of

aluminum, with a thickness of 6 mm, covered by a Ca_2SiO_4 insulator, with a thickness of 30 mm. A Yihua® 992DA+ heated air injector was installed to blow hot air inside the chamber, with a maximum temperature of 220°C. One of the issues with the bench was the displacement of the nozzle along the X axis (see Figure 2), constrained by the superior wall of the chamber. This was solved with a system of interlocked blades inspired by the telescopic covers of Computer Numerical Control (CNC) systems.

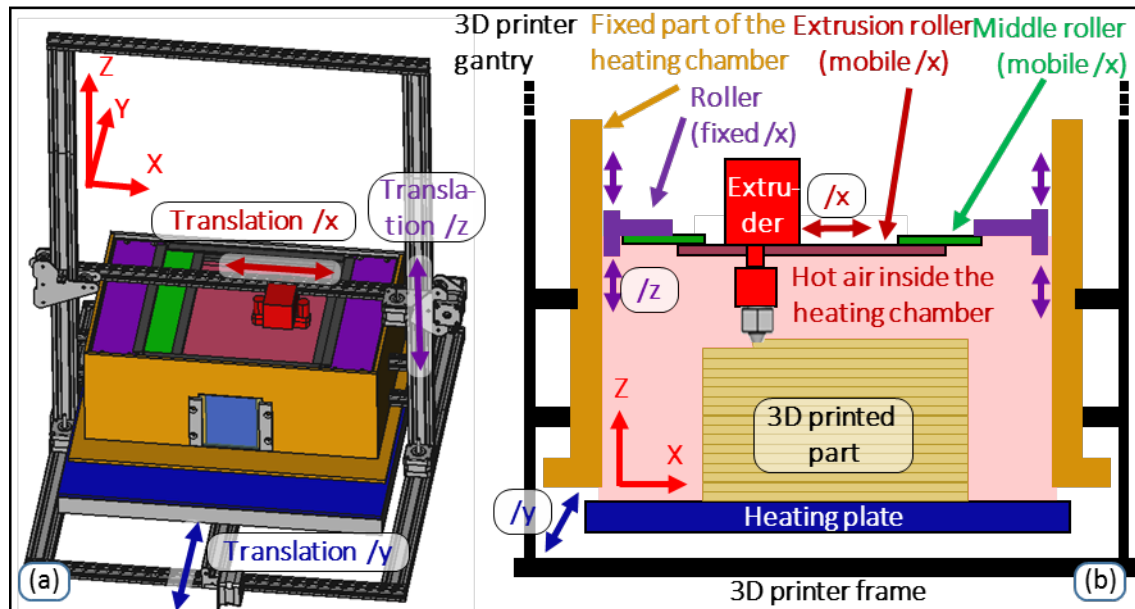


Figure 2 – The instrumented bench designed and manufactured to investigate heat transfer at the filament scale. (a) CAD of the experimental bench showing the three displacement directions (b) a 2D cross-sectional diagram.

2.3.2. Measurement strategy

In the experimental bench, the temperature of the polymer is assessed by measuring the flux emitted by radiation with an IR camera (see Figure 3). This method offers the advantage of being non-intrusive but has the drawback of producing an indirect measurement because the emitted flux then has to be converted into temperature and can be affected by reflections or partial transmissions.

The instrumentation is composed of an infrared camera to measure the temperature of the extruded filament, and of K-type thermocouples, 125 μm in diameter, to measure the temperature of the air. Two further K-type thermocouples, 80 μm in diameter, are also used to check the temperatures imposed for the nozzle and heating plate. Data is acquired with a cDAQ-9171 and a TB-9212 from National Instruments®. The IR camera used is an FLIR SC7500 InSb, with 320×256 pixels on a maximum frequency of 320 Hz for the $\lambda = 1.5\text{--}5.1 \mu\text{m}$ wavelength range [46]. An MW G1 F/3.0 objective is used [47], with a resolution of 0.030 mm/pixel. The specifications only indicate 70% transmission on the wavelength range $\lambda = 3.7\text{--}5.1 \mu\text{m}$. An IR-transparent window in CaF_2 material was chosen to keep the heating chamber closed and insulated.

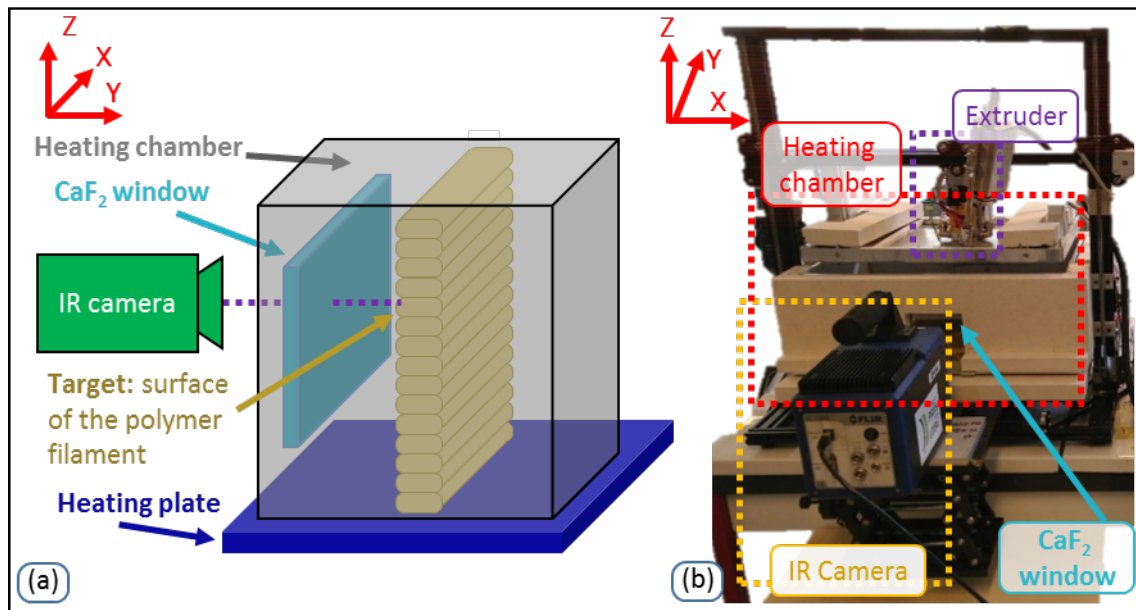


Figure 3 – Temperature measurement of the filaments during deposition using an IR camera: (a) side view 3D schema, (b) front view.

Infrared technology for measuring temperatures is highly sensitive to the emissivity of the material. To ensure measurement accuracy, the absorbance of the polymer was measured at ambient temperature in the mid-IR wavelength range (Table 1). To obtain absorbance, the normal-hemispherical transmittance and reflectance were characterized, absorbance being directly linked to the emissivity of the material according to Kirchoff's law. An FTIR spectrometer (Fourier Bruker Vertex 80V) was used, with a golden integrating sphere, KBr separator, and LN-MCT Mid detector.

Material	Absorbance on	Absorbance on	Repeatability
	$\lambda = 1.5\text{--}5.1 \mu\text{m}$ (IR camera)	$\lambda = 3.7\text{--}5.1 \mu\text{m}$ (IR camera objective)	
Amorphous PEKK 6004	0.75 ± 0.01	0.91 ± 0.004	6 measurements on 3 samples
Semi-crystalline PEKK 6004	0.80 ± 0.06	0.91 ± 0.02	2 measurements on 1 sample

Table 1 – Measured radiative properties of PEKK KEPSTAN™ 6004.

The high absorbance values of the material and, therefore, of its emissivity indicate that an IR camera is suitable to measure the temperature of the polymer. However, the emissivity of the material is not the only information necessary to obtain the temperature of the printed filament. When the IR camera is used, the radiative heat flux measured is affected by several phenomena, (i) partial transmission through the lens ($>70\%$ on $\lambda = 3.7\text{--}5.1 \mu\text{m}$), (ii) partial transmission through the CaF_2 window (95% on $\lambda = 1.5\text{--}5.15 \mu\text{m}$ and 96% on $\lambda = 3.7\text{--}5 \mu\text{m}$) and (iii) multiple reflections from the environment (nozzle, plate, heating chamber walls) on the polymer. To take into account the partial transmissions, a calibration procedure is then used, where the surface temperature of a PEKK sample is simultaneously measured by the IR camera and by thermocouples, as presented in Figure 4. The homogeneous heating of the sample is ensured by an axial furnace, from 90 to 360°C, in which the same CaF_2 IR-transparent window is installed. A conversion law between the digital level of the IR sensors (in counts) and the surface temperature of the polymer (in °C) was obtained for several integration times configured in the IR camera

(Figure 4b). The setup is representative of the printing chamber in terms of material, environment, optical path and temperatures. The sensitivities of the obtained calibration (between 25 and 200 counts per degree) validates the adequacy of the IR measurement technique for temperature measurement.

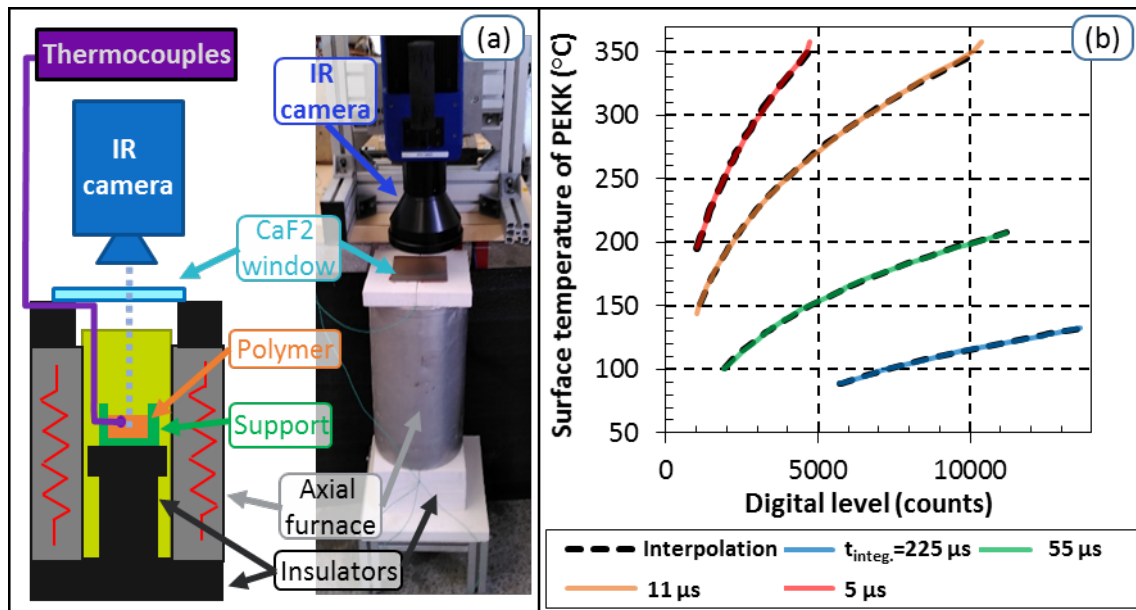


Figure 4 – IR camera calibration: (a) description of the apparatus and (b) equivalence between surface temperature (in °C) and digital level of the IR camera sensors (in counts).

3. Physics modelling and simulation models

3.1. Heat transfer modelling

This section covers modelling of heat conduction in the filament during the FFF process. The fixed domain used is shown in Figure 5 for a wall made with a single filament in the thickness. The transient heat equation can be solved to obtain the temperatures and the heat fluxes in a section. The exothermic source term is not considered because of the low and slow crystallization mentioned above. Initial temperature $T_{extrusion}$ is imposed by the extruder (domain 4 in Figure 5). The filament is then cooled by convection and radiation with the surrounding air at $T_{chamber}$, (domain 1 in Figure 5), and by conduction with the previously extruded filament (boundary 2 in Figure 5). The lower face of the support plate is maintained at T_{plate} (domain 5 in Figure 5). The thermal contact resistances between filaments also affect the conductive transfer (boundaries 2 and 3 in Figure 5).

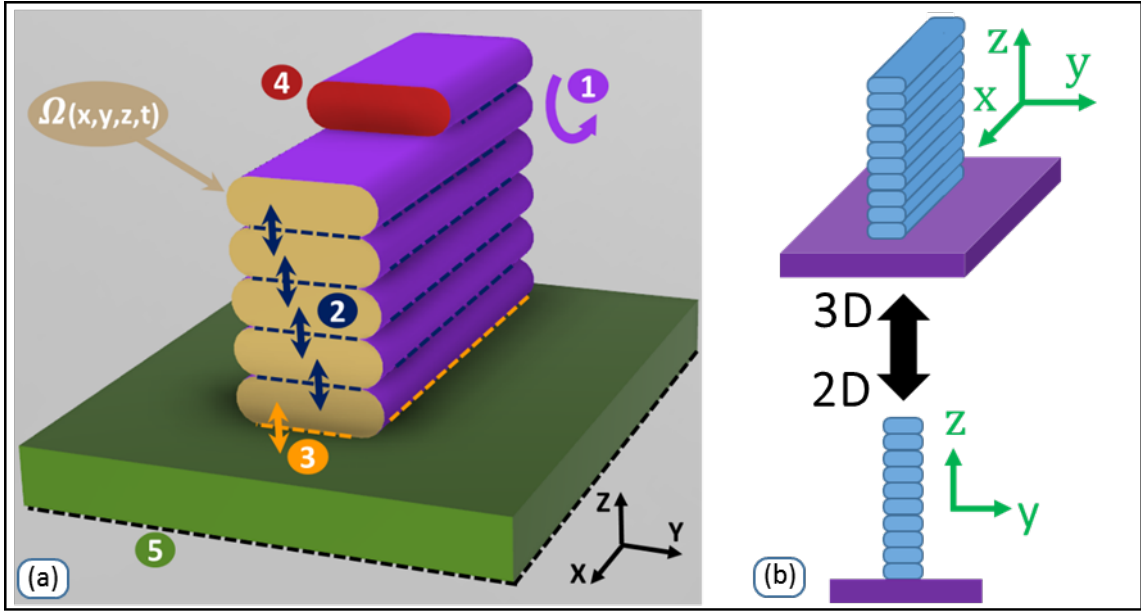


Figure 5 – Heat transfer modelling for the FFF process: (a) domain and boundaries and (b) simplification from 3D to 2D.

As mentioned in a previous study [48], the heat transfer equation can be written with dimensionless numbers:

$$\frac{\partial T^*}{\partial t^*} = Fo_x \frac{\partial^2 T^*}{\partial x^{*2}} + Fo_y \frac{\partial^2 T^*}{\partial y^{*2}} + Fo_z \frac{\partial^2 T^*}{\partial z^{*2}} \quad (1)$$

introducing the three Fourier dimensionless numbers:

$$Fo_x = \frac{k \tau_c}{\rho c_p L_x^2} \quad Fo_y = \frac{k \tau_c}{\rho c_p L_y^2} \quad Fo_z = \frac{k \tau_c}{\rho c_p L_z^2} \quad (2)$$

with $T^* = (T - T_{\text{chamber}}) / (T_{\text{extrusion}} - T_{\text{chamber}})$ the dimensionless temperature, $t^* = t / \tau_c$, τ_c the dimensionless time, which is a chosen characteristic time of the process, $L_x(t)$ the length of the extruded filament, L_y the width of the filament section, L_z the height of the filament section, ρ the density, and C_p the specific heat. The polymer material is considered as isotropic with k , the thermal conductivity.

As stated in the literature [13], the longitudinal conductive heat flux along the direction of the filament can be ignored, although the physical condition was not given in the previous study in question. This simplification condition is given by the non-dimensional analysis of the heat transfer governing equation. The conductive heat flux in the x direction must be negligible with respect to the fluxes in the y and z directions. This can be written as:

$$Fo_x \ll \min(Fo_y; Fo_z) \quad (3)$$

and, by arbitrary choice, can also be considered as:

$$Fo_x < 0.05 \times \min(Fo_y; Fo_z) \quad (4)$$

Because the height of the filament section, L_z , is smaller than the width, L_y , the relation $Fo_y < Fo_z$ is validated. Therefore, the simplification condition from Equation (4) can also be written in terms of position or printing time for a given filament n :

$$L_x > 2\sqrt{5} \times L_y \quad \text{or} \quad t_{n^{\text{th}} \text{ filament}} > 2\sqrt{5} \times L_y / v_{\text{nozzle}} \quad (5)$$

where $v_{\text{nozzle}} = L_x / t_{n^{\text{th}} \text{ filament}}$ is the velocity of the nozzle and $t_{n^{\text{th}} \text{ filament}}$ starts at 0 s at the deposition of each new filament.

In our experimental case, the section filament width is $L_y = 2.5$ mm and the nozzle velocity is $v_{\text{nozzle}} = 8$ mm/s. The 3D to 2D simplification is then validated for $L_x > 11.2$ mm or $t > 1.4$ s, which are realistic experimental conditions.

This Lagrangian model of the heat conduction in the filament during the FFF process can now be solved with a numerical tool.

3.2. Heat transfer method

COMSOL Multiphysics® 5.6 finite element software was used to solve the non-linear conduction problem shown in Figure 6 (a). The model is implemented with the following characteristics.

- A wall with 2D geometry is considered, being a single filament in thickness and 15 filaments in height. This simplification is valid as long as Equation (4) is validated.
- A multistep approach is used for successive filament deposition. At each step, the geometry is appended with a new filament by "domain activation". The new filament is initially at extrusion temperature and the previous filaments are initially at the final temperature of the previous step (see Figure 6 (b)).
- Time integration is implicit, with an auto-adaptive time step from the built-in solver (around 30 calculations per deposition step).
- Space integration is done with finite elements, using around 400 quadratic triangular elements for temperature discretization.

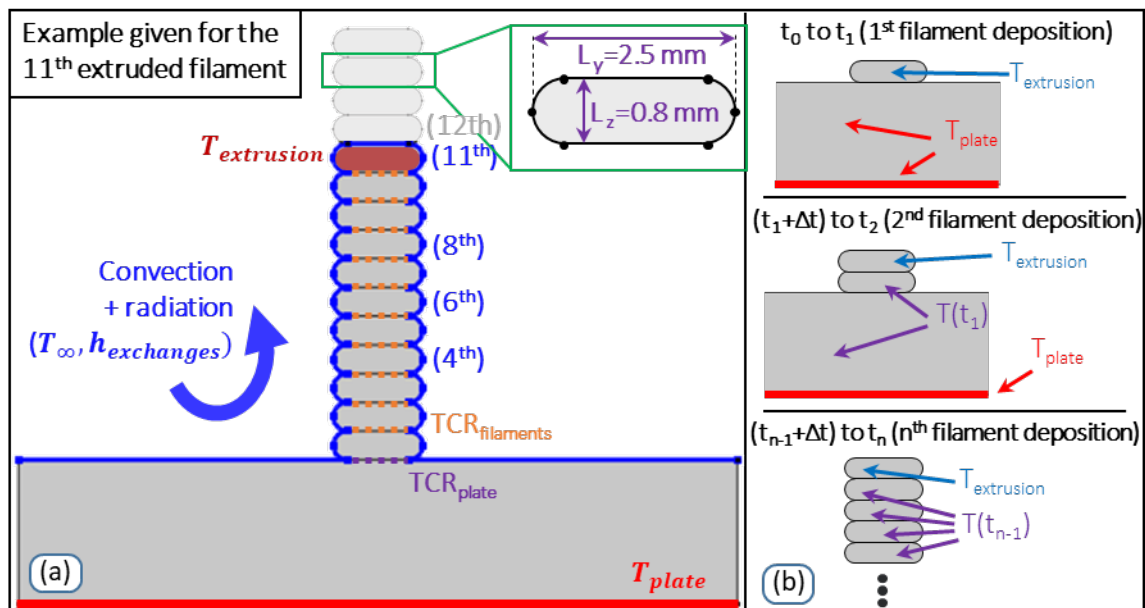


Figure 6 – Numerical implementation in COMSOL Multiphysics®: (a) 2D model description and (b) initial temperature conditions imposed for each new filament deposition.

The heat equation is solved for the filaments and the support plate. The different conditions are given as:

- Boundary conditions: convection and radiation with the environment at T_∞ are described by a single heat transfer coefficient $h_{exchange}$. The temperature of the environment is variable according to experimental observations. A thermocouple is placed in front of the nozzle, measuring the chamber temperature. It follows the nozzle displacement, and the results show temperature variations of $\pm 15^\circ\text{C}$ near the filament for an average chamber temperature of 138°C [49].
- Interface conditions: internal thermal contact resistances are imposed between the plate and the first filament TCR_{plate} and between each filament $TCR_{filaments}$.
- Initial conditions: extruded filament temperature is set at $T_{extrusion}$, the lower boundary of the support plate is maintained at T_{plate} and temperature of the rest of the structure is taken from the previous deposition step at $T(\text{filament } n)_{ini} = T(\text{filament } n-1)_{end}$ (see Figure 6 (b)).

The reference parameters used in this model are given in Table 2.

Reference parameters	Value
Extrusion temperature	340°C
Support plate temperature	140°C
Heating chamber temperature	130°C to 145°C
Convection heat transfer coefficient	$50 \text{ W/m}^2\cdot\text{K}$
Thermal contact resistance plate-first filament	$5 \times 10^{-5} \text{ m}^2\cdot\text{K/W}$
Thermal contact resistance filament-filament	$1 \times 10^{-4} \text{ m}^2\cdot\text{K/W}$
Time between two depositions	30 s
Oblong geometry for the filament section	width: $L_Y = 2.5 \text{ mm}$, height: $L_Z = 0.8 \text{ mm}$

Table 2 – Modelling parameters considered for the numerical study.

3.3. Adhesion model

The adhesion of two filaments printed with the FFF process involves two phenomena: coalescence and interface healing [10,12]. We propose models to predict the degrees of each of these phenomena.

3.3.1. Coalescence model

As illustrated in Figure 1 (a), the coalescence model describes the temporal evolution of the geometry of two filaments in contact. With the objective of predicting the contact angle $\theta(t)$, the model is based on Frenkel-Eshelby's approach [27,28] but applied to a cylindrical section [45]. This model was first used by Hirao and Tomozawa [50] and was fully formulated by Defauchy [51]. It considers (i) an incompressible Newtonian viscous fluid, (ii) an isolated system without any exterior forces (contact, gravity, pressure) but with the surface tension and (iii) a uniform deformation in the system. More recent studies present the coalescence by solving the Navier-Stokes equations [34–36], which is more robust but also more costly in computation time. Even though Frenkel-Eshelby's model considers the coalescence of spheres, it is able to predict the coalescence of two molten polymer cylinders inside an oven [9,10,33]. However, this model becomes less accurate at predicting experimental data of

FFF printed filaments [32]. This difference arises either from an erroneous estimation of the interface temperature of the filaments or from the strong model assumptions mentioned above.

The obtained constitutive equation for the coalescence rate is:

$$\frac{d\theta}{dt} = A(T) \times B(\theta) \quad (6)$$

where θ is the contact angle of the two cylinders in coalescence.

$$A(T) = \gamma(T) / (\mu_0(T) \times a_0) \quad (7)$$

is a function linked to the physical properties of the material, with $\gamma(T)$ the surface tension of the polymer, $\mu_0(T)$ the Newtonian viscosity of the polymer, and a_0 the initial radius of the two cylinders.

$$B(\theta) = \frac{1}{2\sqrt{\pi}} \frac{(\cos\theta + \sin\theta / (\pi - \theta)) \times \cos\theta \times (\pi - \theta + \cos\theta \sin\theta)^{0.5}}{\sin^2(\theta) \times (\pi - \theta)} \quad (8)$$

is a function only linked to the geometry of the entities in coalescence.

The link between the coalescence angle $\theta(t)$ and the interface half-length $x(t)$ shown in Figure 1 (a), is:

$$x(t) = \sin\theta \times a(t) = \sin\theta \times a_0 \times \pi^{1/2} \times (\pi - \theta + \cos\theta \times \sin\theta)^{-1/2} \quad (9)$$

The degree of coalescence for two cylinders in coalescence is then defined as:

$$D_{coalescence} = x(t) / (\sqrt{2} a_0) \quad (10)$$

In order to predict the coalescence evolution for filaments printed with FFF, the evolution equation (6) should be integrated. Therefore, under non-isothermal conditions, it is necessary to:

- Consider the thermal history at the interface of the printed filaments in order to know the corresponding evolutions of the properties during the printing of the part.
- Know the evolution of the physical properties involved in coalescence: the viscosity and surface tension, considering their temperature dependency.
- Consider a coalescence model for cylinders (Defauchy) rather than for spheres (Frenkel-Eshelby).

3.3.2. Interface healing model

Once the coalescence process has started, the contact between the two entities to be welded is made, but the bond is initially weak. The healing of the interface then begins, as illustrated in Figure 1 (b). Macromolecular polymer chains will interdiffuse on each side of this interface, which will gradually develop bond strength. This polymer chain motion can be described with the de Gennes reptation theory [37].

The interface is considered totally healed when the mechanical resistance there becomes equal to the resistance of the bulk material [4,52]. The time required to achieve a fully healed interface is the material welding time, which is lower than or equal to the material reptation time [53,54]. This welding time is strongly dependent on the temperature and can be determined mechanically [4,52,54,55]. The welding time will be assumed to be equal to

the longest relaxation time, which can be determined through a rheological characterization. Thus, the degree of healing can be deduced from the longest relaxation time $t_R(T)$ with [4, 54]:

$$D_{healing} = \left(\frac{t}{t_R(T)} \right)^{1/4} \quad (11)$$

The temperature taken into account is located at the interface of two filaments. To be solved for anisothermal conditions, Equation (11) can be written in its differential form. With a variable change $C = D_{healing}^4$ and a simplification, it can be written as:

$$\frac{dC}{dt} = \frac{1}{t_R(T)} \quad (12)$$

An explicit numerical scheme was chosen for the integration, leading to:

$$[D_{healing}]_{t+1} = \left(\frac{\Delta t}{t_R([T]_t)} + [D_{healing}]_t \right)^{1/4} \quad (13)$$

In order to predict the interface healing evolution, the following are required:

- The thermal history $[T]_t$ at the interface of the printed filaments, as for the coalescence.
- The evolution of the longest reptation time $t_R(T)$ considering the temperature dependency.

4. Results and discussion

4.1. Heat transfer study of the FFF process

4.1.1. Experimental study

Temperature measurements were made using the IR camera on the experimental bench during the printing of the part with PEKK. The geometry chosen was still a wall, a single filament thick, with a height and a width equal to 40 mm. The filament section height and width were the same as for the numerical analysis. The imposed temperatures for the process were 360°C for the nozzle, 140°C for the heating plate, and 180°C for the heating tool. New filaments were deposited every 30 s.

The results of the temperature measurements are shown in Figure 7. The measurement was performed on an area of $9.6 \times 7.7 \text{ mm}^2$ that was distant enough from the edge of the part to respect the condition mentioned with Equation (5). At $t = 0 \text{ s}$, a stack of filaments had previously been deposited and was, therefore, already cold. Figure 7 then shows $t = 2.0, 2.5,$ and 3.0 s , as the filament is extruded (Figure 7). Then, from $t = 4.0 \text{ s}$ to 20.0 s , the filament cools down. The initial temperature of the deposited polymer can be seen in red, just after the extrusion of the filament. The heat is first concentrated on the extruded filament, and is then diffused to the previously deposited filaments, shown in green at $t = 4.0, 5.0,$ and 10.0 s . The polymer then reaches a more homogenous thermal state during its cooling, as can be seen at $t = 20.0 \text{ s}$. This trend is in agreement with previously observed experiments [22, 26, 60].

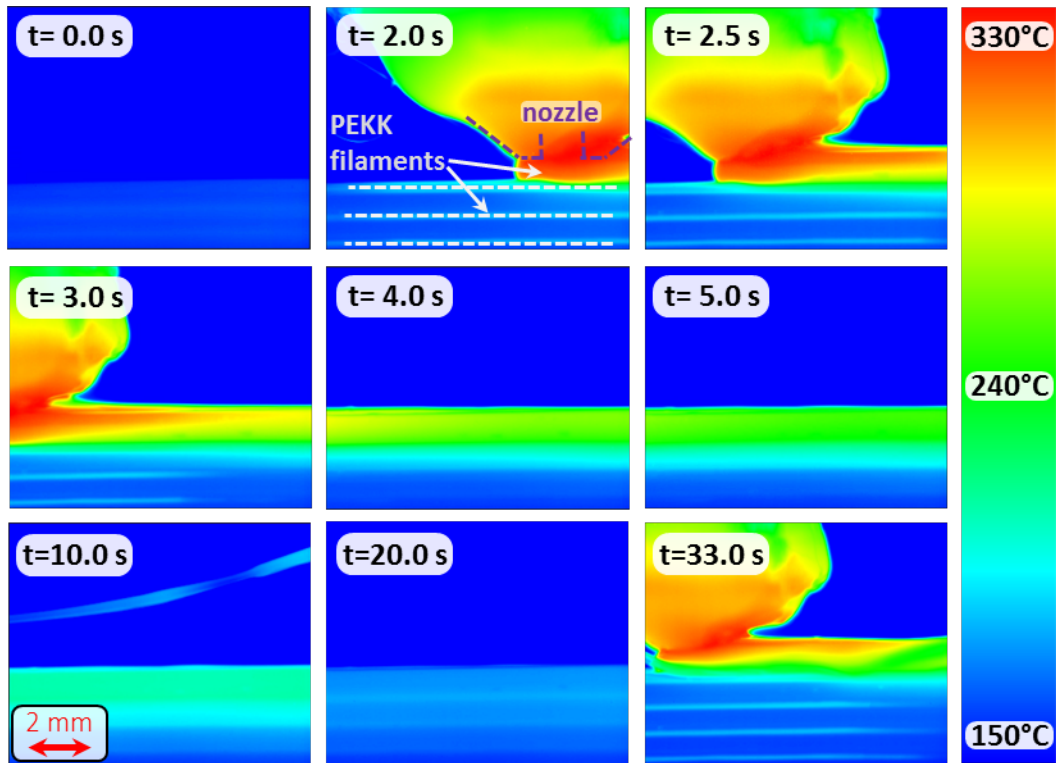


Figure 7 – Thermograms obtained with the IR camera for two successive depositions of PEKK material filaments, with 30 s between two depositions.

At $t = 2.0, 2.5, 3.0,$ and 33.0 s, some glowing horizontal lines can be seen, which correspond to the interfaces of the filaments. These lines only appear when the nozzle is moving above. With different situations observed, it was found that this phenomenon is due to reflection from the nozzle to the polymer. This is in conjunction with the curvature effect mentioned by Seppala & Migglér [24].

The thermograms obtained with the IR camera were post processed with ResearchIR[®] software from FLIR[®]. The temperature evolutions, plotted in Figure 8, were obtained based on the calibration curves presented in Figure 4 (b). The temperatures considered were averaged from an area of 1 pixel in width and 13 pixels in height, equal to 0.4 mm, which corresponds to half of the filament height. We thus obtained a measurement with more reliability and avoided the influence of a potentially defective pixel. For printing conditions with 26 s between each filament instead of 30 s, the extracted temperatures are plotted versus time in Figure 8 for different layer heights through the stack of 50 filaments. The two printing conditions (Part A and B) are summarized in Table 3. Note that the extrusion temperatures are that of the polymer, obtained from the IR camera measurement, and differ from the printer setpoint which is the temperature of the heating element. The difference might be important in the case of large flowrate when the polymer does not reach steady state temperature in the nozzle.

Parameter	Part A	Part B
Extrusion temperature $T_{\text{extrusion}}$ (°C)	329	317
Support plate temperature T_{plate} (°C)	138	138
Environment temperature T_{∞} (°C)	Cycles between 130 and 145°C	Cycles between 128 and 146°C

Time between two filament depositions $t_{\text{depositions}}$ (s)	30	15
Length and width of the oblong filament section $L_y \times L_z$ (mm ²)	2.4×0.8	2.4×0.8
Thermal contact resistance $\text{TCR}_{\text{filaments}}$ (m ² ·K/W)	1×10 ⁻⁴	1×10 ⁻⁴
Thermal contact resistance $\text{TCR}_{\text{plate}}$ (m ² ·K/W)	5×10 ⁻⁵	5×10 ⁻⁵

Table 3 – Parameters used in the simulation corresponding to parts A and B fabricated with the experimental bench.

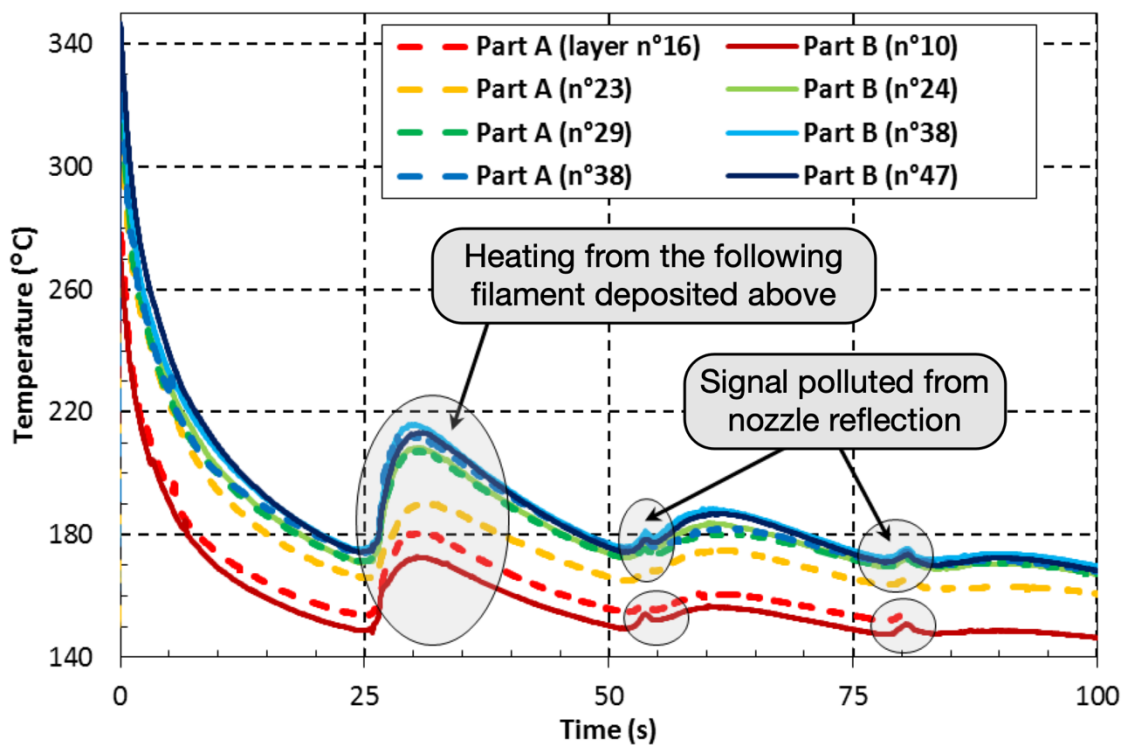


Figure 8 – Temperature versus time, obtained at different layer heights and extracted from two different parts (part A and part B) with the same printing parameters, for a part made of 50 filaments with 26 s between two depositions.

All the curves show the same temperature evolution. The initial temperature corresponds to the extrusion temperature, with a first cooling between 0 and 25 s. At $t = 25$ s, another filament is deposited, triggering a reheating of the previous filament by conductive heat transfer [26]. The same effect, with lower amplitude, can also be seen at $t = 52$ s and $t = 78$ s, still corresponding to new filament depositions. This reheating phenomenon strongly impacts the overall thermal history.

At $t = 52$ s and 78 s, a small heating peak with an amplitude of 3°C appears. This corresponds to a signal disruption brought about by the reflection of the nozzle already mentioned and visible in Figure 7.

For the layers n° 10, 16 and 23 in Figure 8, the temperatures are generally colder than the following layers n° 29 to 47. This phenomenon, identified as a second disruptive signal, must be due to multiple reflections inside the

chamber rather than the heating plate conduction effect. Investigations were carried out revealing that this phenomenon disappears when the temperature is measured with a pyrometer on approximately the same wavelength range, but from above the deposition. The measuring spot of the pyrometer is much smaller and is, therefore, less affected by surrounding reflections. When the extrusion temperatures according to the height of the filament were measured with the pyrometer, the values remained constant, unlike the results shown in Figure 8, with the erroneous measurements of $T_{\text{extrusion}} = 270^{\circ}\text{C}$ for layer n° 10, to $T_{\text{extrusion}} = 347^{\circ}\text{C}$ for layer n° 47.

Above a given layer, named the "threshold layer", the temperature evolution is no longer affected by the height of the filament, as visible for layers n° 38 and n° 47. After this threshold layer, the repeatability becomes very good, with less than 8°C difference between the temperature evolutions of layers n° 29 and n° 47. This is probably due to a radiation effect from the heating plate and bottom of the heating chamber. The measurement methodology is, therefore, validated when the layer considered is above the threshold layer.

4.1.2. Characterization of heat transfer properties

In order to feed the numerical model, the thermal properties were characterized with the protocols described in section 2.2.1 and are given in Table 4.

Property	$T < T_g$	$T > T_g$	Material tested
Density in $\text{kg}\cdot\text{m}^{-3}$	$-0.211 \times T(^{\circ}\text{C}) + 1272.0$	$-0.683 \times T(^{\circ}\text{C}) + 1339.3^{(*)}$	Amorphous PEKK
Specific heat in $\text{J}\cdot\text{kg}^{-1}\cdot\text{K}^{-1}$	$3.211 \times T(^{\circ}\text{C}) + 1054.5$	$3.037 \times T(^{\circ}\text{C}) + 1449.0$	KEPSTAN™ 6004
Thermal conductivity in $\text{W}\cdot\text{m}^{-1}\cdot\text{K}^{-1}$	0.25	Not characterized	Amorphous PEKK KEPSTAN™ 6002

Table 4 – Thermal properties of the polymer. ^(*)The coefficients of the Tait model used are $[b_1, b_2, b_3, b_4, b_5, b_6] = [8.73 \cdot 10^{-4}, 5.06 \cdot 10^{-7}, 5.75 \cdot 10^7, -2.55 \cdot 10^{-3}, 281.4, 6.64 \cdot 10^{-7}]$, as defined in [44].

The measurement of the thermal conductivity was more complicated for the rubbery state because of the high deformation of the injected sample above the glass transition temperature. Nevertheless, the thermal conductivities obtained were equal to $k = 0.24 \text{ W}\cdot\text{m}^{-1}\cdot\text{K}^{-1}$ at 60°C and $0.25 \text{ W}\cdot\text{m}^{-1}\cdot\text{K}^{-1}$ at 100 and 140°C , with an uncertainty of 5%. The thermal conductivity is not affected by the temperature in this range, so the same value of $k = 0.25 \text{ W}\cdot\text{m}^{-1}\cdot\text{K}^{-1}$ will be considered for any temperature.

4.1.3. Comparison of experiment and model

In order to validate the heat transfer model of the FFF process, the simulation results were compared with the experimental ones. Different experimental situations were considered by varying parameters. To simulate the equivalent conditions in the model, the simulation parameters were identified and are given in Table 3. The temperatures were taken from different thermocouples, the time between two filaments was imposed in the GCODE file with manual verification during the printing. Concerning the geometrical parameters, the length and width of the oblong filament section were directly measured from the microscopic section observations. The thermal contact resistance values $\text{TCR}_{\text{filaments}}$ and $\text{TCR}_{\text{plate}}$ were imposed, inspired by the literature on mold-polymer contact [44,56–58], but their effects were almost negligible, as confirmed by a sensitivity analysis.

The temporal changes in the experimental temperatures of parts A and B are compared with the numerical results in Figure 9. The difference between numerical and experimental temperatures is always lower than 10°C. The heating effect caused by the deposition of new filaments every 30 s for part A and every 15 s for part B is also well reproduced by the simulation.

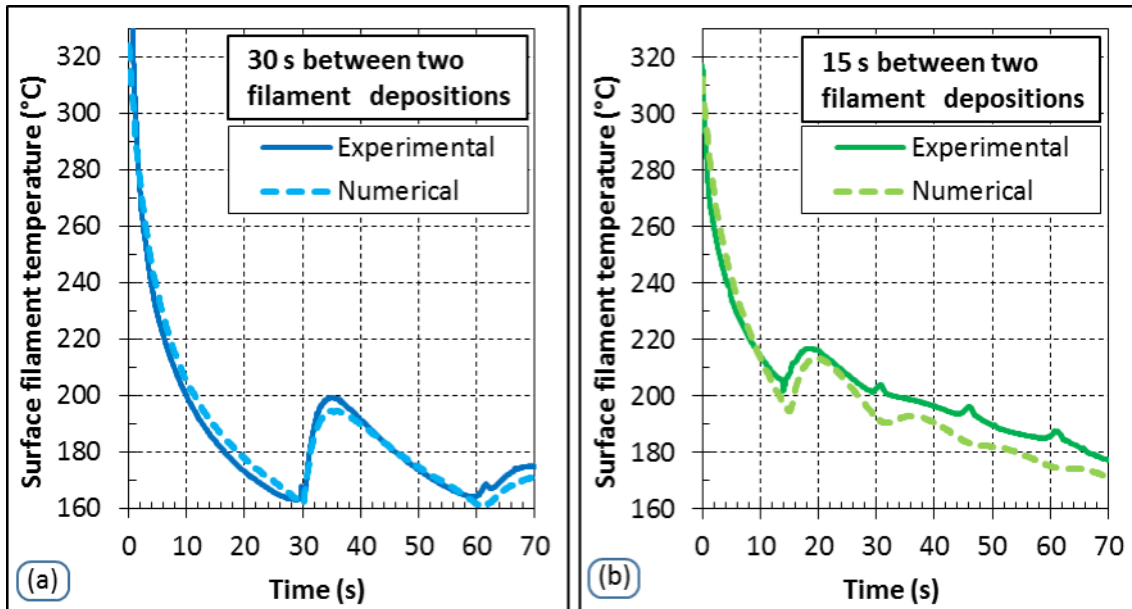


Figure 9 – Surface temperature versus time measured experimentally and predicted numerically. Time between two filament depositions is equal to (a) 30 s for part A and (b) 15 s for part B.

The temperature of the chamber was measured at various locations. Experimental difficulties were encountered with the positioning of the thermocouples because the Z translation system of the experimental bench imposes a chamber height equal to a few mm at the start of printing. Thus, we mainly used one of the thermocouples located in an area close to the nozzle, as shown in Figure 10 (b).

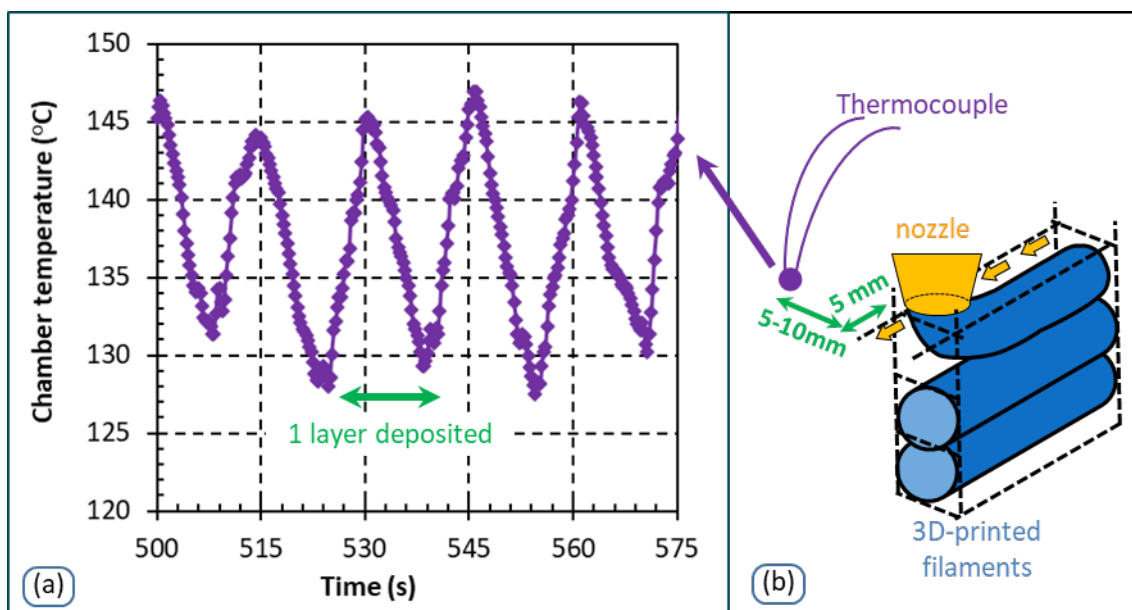


Figure 10 – Thermal heterogeneity inside the heating chamber shown by (a) the temperature fluctuations obtained with (b) a thermocouple placed in the vicinity of the nozzle.

Periodic effects of the rise and fall in temperature can be seen in Figure 10 (a), corresponding to part B in Table 3, with a period corresponding exactly to the time between two successive filament extrusions. The same phenomenon is also observed for the same toolpath when no material is extruded. It, therefore, still occurs without the radiation emitted by the polymer, giving the same cycles but with smaller amplitudes. These experiments suggest that the environmental temperature variation during deposition is due to a mixed effect of convection and radiation from the nozzle and the polymer. As this heat transfer plays a significant role in the cooling of the filaments, these cyclic phenomena were also taken into consideration (see environment temperature in Table 3).

One single overall heat transfer coefficient $h_{\text{exchanges}}=50 \text{ W/m}^2\cdot\text{K}$ can be identified by minimizing the differences between the numerical and experimental temperatures for several experiments. The value of this coefficient corresponds specifically to the situation we have described and depends on the air flow, air temperature and temperature of the filament. For all the following simulation results presented, the heat transfer coefficient remains the same and is equal to this identified value.

4.1.4. Numerical parametric study

With the reference parameters mentioned in Table 2, the temperature evolution was calculated using the simulation tool. The overall cooling of the filaments is shown in Figure 11. The simulation results show the temperature heterogeneity in the filament. Many heat transfer models in the literature consider a small Biot number. This is not validated in our case, and the interface temperature is different from that on the surface (observed with the camera). It confirms the need for a numerical model to estimate the interface temperature.

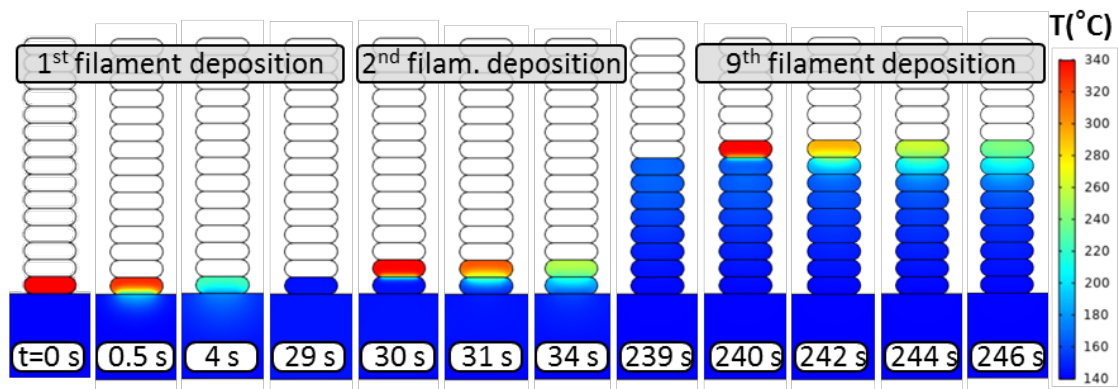


Figure 11 – Simulation of the successive cooling after filaments deposition. The temperature fields show heterogeneity and confirm the necessity of a spatial description (here, with finite elements).

4.1.4.1. Influence of the plate and temperature heterogeneity

The surface temperatures were studied according to the position of the filament in the structure. These are plotted in Figure 12 (a). Time is shifted in order to match the different temperature evolutions at $t = 0 \text{ s}$. The temperature change of the first filament shows a sudden cooling between 0 and 20 s, due to contact with the plate, which is colder ($T_{\text{plate}} = 140^\circ\text{C}$) than the extruded polymer ($T_{\text{extrusion}} = 340^\circ\text{C}$). The higher the filament is located in the structure, the less the plate influences the cooling [12,13,16,26]. Therefore, the influence of the support plate

becomes negligible from the 8th filament. To describe a typical printing situation, all the simulations considered hereon will consider filaments above this number, to avoid the influence of the heating plate.

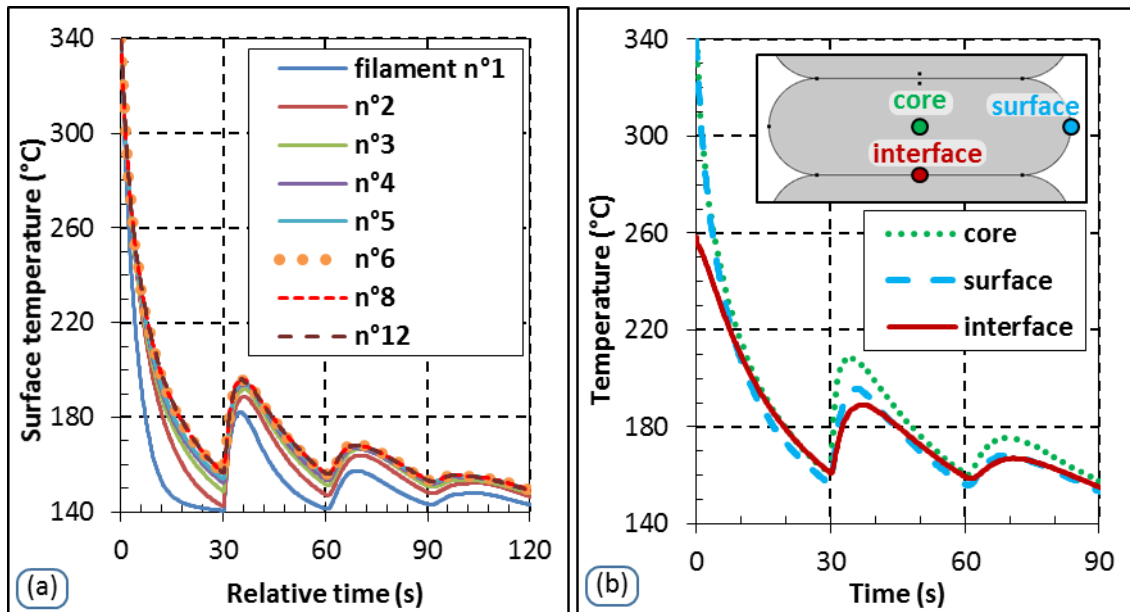


Figure 12 – Simulated temperature evolution: (a) at the surface, showing the influence of the heating plate and repetitive cooling after the 8th filament; and (b) at different locations within the filament, showing the thermal heterogeneity in the filament section during its cooling.

Figure 12 (b) shows the thermal heterogeneity, with a gradient within the filament section. The temperatures were studied at three points located at the core and on the surface of the 11th filament, and at the interface between the 10th and the 11th filament. With the filament geometry used in this study (oblong section: 2.5 mm width by 0.8 mm height), the core and surface points were generally hotter than the interface due to thermal shock caused at the interface by the contact of the newly extruded filament with the previous one. Some simulation results showed different conclusions for smaller filaments. Otherwise, the point on the surface cooled slightly faster than the one at the core, due to exchange with the environment. This result shows the importance of using the interface temperature in order to study the adhesion between two filaments, t (see Figure 12 (b)). This interface temperature can only be obtained with a predictive model, because of the difficulties of instrumenting this area without intrusiveness.

4.1.4.2. Contributions of the different heat transfers

The predominant heat transfer mode during cooling was studied by comparing the heat transferred by: (i) conduction between a deposited filament and the one below it, and (ii) convection and radiation. The simulation uses the reference parameters previously presented in Table 2. For a given filament, the contributions of each of the two fluxes versus time are plotted in Figure 13 (a). Because the geometry is 2D, heat fluxes are given by unit length.

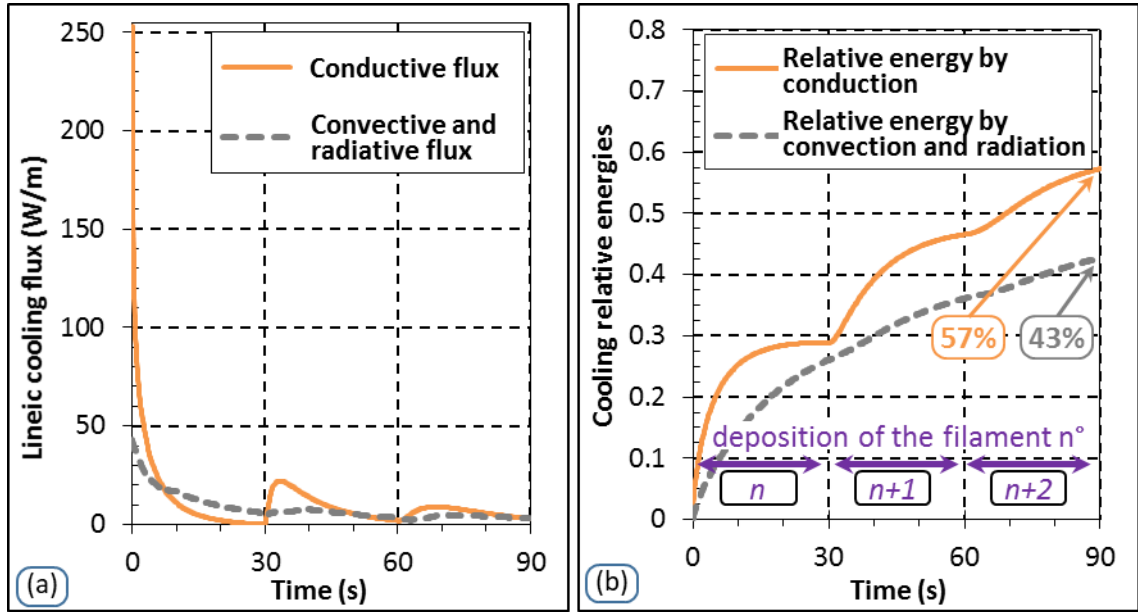


Figure 13 – Energy repartition by type of heat transfer with (a) cooling flux evolution and (b) the corresponding relative energies during 90 s of cooling.

To compare the two fluxes, the relative thermal energies are calculated from the outward fluxes normalized on the corresponding boundaries by conduction, $\Phi_{cond.}$, and by convection and radiation, $\Phi_{conv.+rad.}$, as:

$$E_{r,cond.} = \int_{t_0=0s}^t \Phi_{cond.}(t) dt / \int_{t_0=0s}^{t_{final}=90s} [\Phi_{cond.}(t) + \Phi_{conv.+rad.}(t)] dt \quad (14)$$

$$E_{r,conv.+rad.} = \int_{t_0=0s}^t \Phi_{conv.+rad.}(t) dt / \int_{t_0=0s}^{t_{final}=90s} [\Phi_{cond.}(t) + \Phi_{conv.+rad.}(t)] dt \quad (15)$$

where $E_{r,cond.}$ and $E_{r,conv.+rad.}$ are the relative cumulated energies transferred by conduction, and by convection and radiation, respectively; t_0 is the initial time when the filament is extruded; and t_{final} the final time considered, equal to $(t_0 + 90)$ s in our case.

These energies are plotted against time in Figure 13 (b). The cooling energy by conduction appears slightly higher than the convective and radiative effects. At the end of the period ($t = 90$ s), the ratios indicate that the filament is cooled 57% by conduction and 43% by convection.

As these contributions are comparable, both of the fluxes must be taken into consideration to study the overall cooling. Once again, this shows the limitation of lumped-capacity 1D models that do not take into account the conduction between the filaments.

4.2. Adhesion study for the FFF process

The coalescence and interface healing models were used to predict the adhesion quality of the printed parts. Those models needed knowledge of the viscosity, surface tension, and relaxation time, all of which were characterized with taking temperature dependency into consideration.

4.2.1. Characterization of the properties linked to adhesion

With the protocols described in section 2.2.2, the properties used to model the coalescence were characterized and are given in Table 3.

Property	$T < T_g$	$T > T_g$
Surface tension in $N \cdot m^{-1}$	$-3.0 \cdot 10^{-5} \times T(^{\circ}C) + 4.43 \cdot 10^{-2}$	$-6.1 \cdot 10^{-5} \times T(^{\circ}C) + 4.90 \cdot 10^{-2}$
Newtonian viscosity in $Pa \cdot s$	Solid state	$2.07 \cdot 10^{-6} \times \exp\left(\frac{95415}{R \times T(K)}\right)$

Table 3 –Physical properties of the polymer required to model coalescence for PEKK KEPSTAN™ 6004 [45].

Additionally, also with the procedure described in section 2.2.2, the longest relaxation time, required to model the interface healing, was characterized and is given in Table 4.

Property
Relaxation time in s
$2.04 \cdot 10^{-4} \times \exp\left(\frac{43970}{R \times T(K)}\right)$

Table 4 – Longest relaxation time of PEKK KEPSTAN™ 6004.

4.2.2. Adhesion study: coalescence and interface healing

The overall adhesion can be estimated with the degree of coalescence from Equation (10), which assesses the collapse of the macroporosities between the filaments, and the degree of healing from Equation (11), which evaluates the quality of the bond at the interface. A maximum degree of coalescence $D_{coalescence} = 1$ is not wanted, because it would correspond to a coalescence angle of $\theta = 90^{\circ}$ (see Figure 1), thus forming a single cylinder from two filaments. Even if the adhesion quality would be better, mechanically speaking, with a higher D_c , the geometrical definition of the printed part might not be respected.

From the typical thermal history at the interface of two filaments given in Figure 14 (a), which was obtained with reference parameters from Table 2, the degree of coalescence and degree of healing were calculated with the models presented above and are plotted in Figure 14 (b).

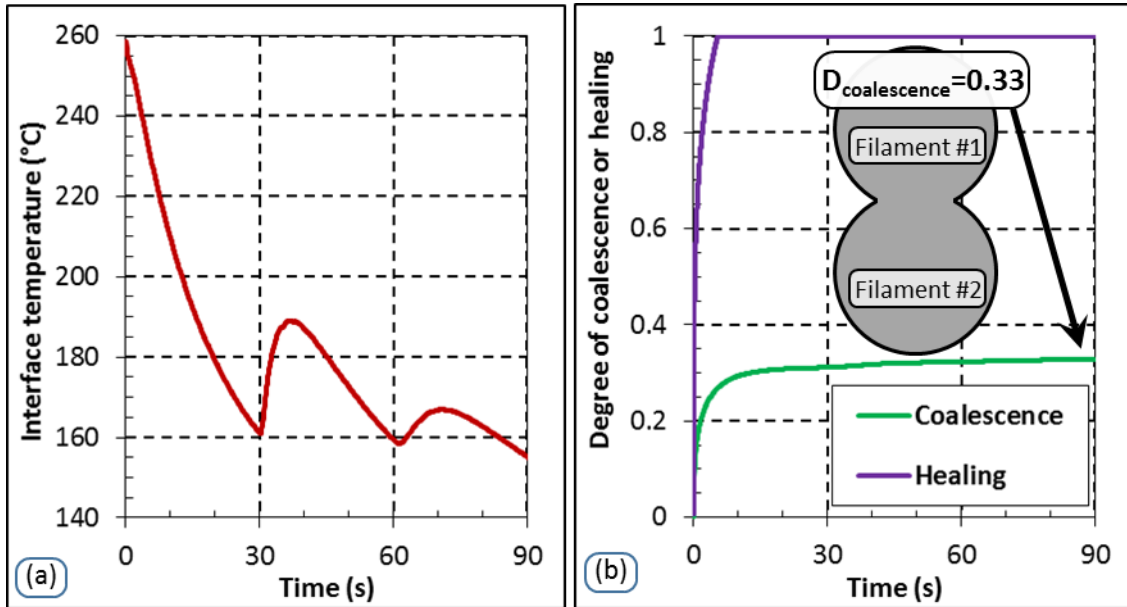


Figure 14 – (a) Temporal evolution of the temperature for PEKK extruded material, used to calculate (b) the degree of coalescence and degree of healing between two filaments.

The degree of coalescence increases fast at the beginning, to reach an asymptotic value of $D_{coalescence} = 0.33$ (see Figure 14). To describe this evolution, the material component $A(T)$ in Equation (7) varies by two orders of magnitude during the 90 s considered for filament deposition. However, the geometrical component of the coalescence model, $B(\theta)$ in Equation (8), has an infinite value during the very first instants, because of the mathematical singularity at $\theta = 0$, and stabilizes after a few seconds at a value that does not vary much until the final degree of coalescence. The coalescence evolution is, therefore, mainly controlled by the evolution of properties from $A(T)$, and in this case, by the high increase of the viscosity [45] at low temperatures.

The degree of healing reaches its maximum value $D_{healing} = 1$ after 5 s. This fast interface healing comes from the very short relaxation time of the PEKK KEPSTAN™ 6004. Note that the values of the relaxation times were obtained at higher temperatures, from 340 to 380°C, and fitted with an Arrhenius law. The WLF model was not chosen here because it is only valid for lower temperatures ($T_g < T < T_g + 100^\circ\text{C}$), and the characterization at temperatures below 260°C was experimentally too difficult to perform because of the high viscosity of the polymer and the starting of the crystallization process.

4.2.3. Decision tool for adhesion in isothermal conditions

For isothermal conditions, the two models of coalescence and interface healing can be used to establish time-temperature-coalescence (TTC) and time-temperature-healing (TTH) diagrams that provide precious information about the adhesion for the final user. Figure 15 presents these diagrams, with the iso-values of the degrees of coalescence and healing at given temperatures for given times. The TTC diagram is given, in this case, for an initial radius of the cylinder $a_0 = 0.77 \text{ mm}$, which is equivalent to an oblong filament section with $L_y = 2.5 \text{ mm}$ and $L_z = 0.8 \text{ mm}$ considering iso-area (description in Figure 6). The two diagrams use the characterized viscosity, surface tension, and relaxation times for PEKK KEPSTAN™ 6004.

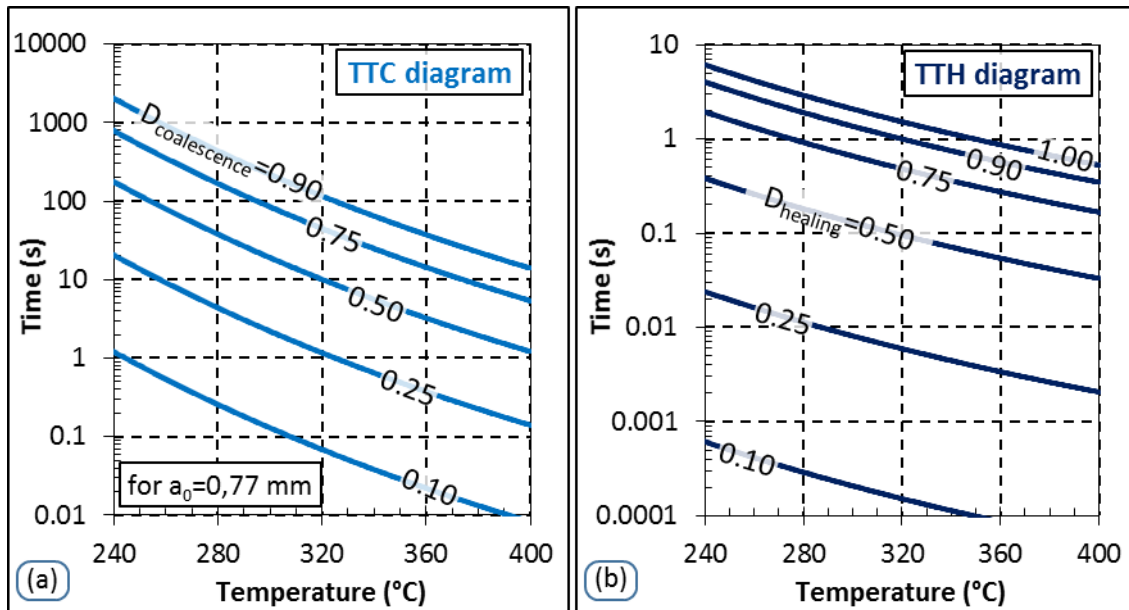


Figure 15 – For isothermal conditions, the (a) time-temperature-coalescence (TTC) diagram and (b) time-temperature-healing (TTH) diagram.

Using the TTC and TTH diagrams, if we consider two filaments in contact for 1 s at 320°C, for example, 25% of the coalescence and 90% of the healing will be achieved. Another way to use these diagrams is consider that in order to complete 50% of the coalescence process, for example, the filaments need 10 s contact at 320°C or 80 s contact at 260°C. Even though this tool only considers isothermal conditions, it is very useful for the final user because it gives an order of magnitude of the conditions needed to achieve a specific adhesion.

4.2.4. Parametric study on FFF printing parameters in non-isothermal conditions

In order to help the industrial user understand the influence of each parameter, a parametric study was also carried out on chosen parameters of the FFF process: the time between two successive depositions, the extrusion temperature, and the heating chamber temperature, as presented in Table 5. The interface temperatures were first obtained with the heat transfer model (Figure 16 (a)). They were then post processed to obtain the evolutions of the degrees of coalescence and healing with time (Figure 16 (b)). The final values of the degrees of coalescence and healing are given in Table 5.

<u>Situation</u>	<u>Parameters</u>			<u>Results</u>	
	<u>Time between two depositions</u>	<u>Extrusion temperature</u>	<u>Heating chamber temperature</u>	<u>Final degree of coalescence</u>	<u>Final degree of healing</u>
Case 1 (reference)	30 s	340°C	130 to 145°C	0.22	1 after 5.4 s
Case 2	15 s	340°C	130 to 145°C	0.28	1 after 1.6 s
Case 3	60 s	340°C	130 to 145°C	0.19	1 after 7.2 s
Case 4	30 s	300°C	130 to 145°C	0.17	1 after 10.4 s
Case 5	30 s	380°C	130 to 145°C	0.28	1 after 3.1 s
Case 6	30 s	340°C	90 to 105°C	0.15	1 after 10.4 s
Case 7	30 s	340°C	50 to 65°C	0.11	1 after 106.5 s

Table 5 – Parametric study: parameters tested to calculate the interface temperature, post processed to obtain the corresponding final degree of coalescence and degree of healing.

For all the situations, full healing ($D_{\text{healing}} = 1$) is reached, but at different times, from 1.6 to 106.5 s. The final degrees of healing are not proportional to the final degrees of coalescence, showing the different kinetics of the two phenomena. Again, these results are linked to the short relaxation times of PEKK KEPSTAN™ 6004. The overall adhesion is thus limited by the coalescence process.

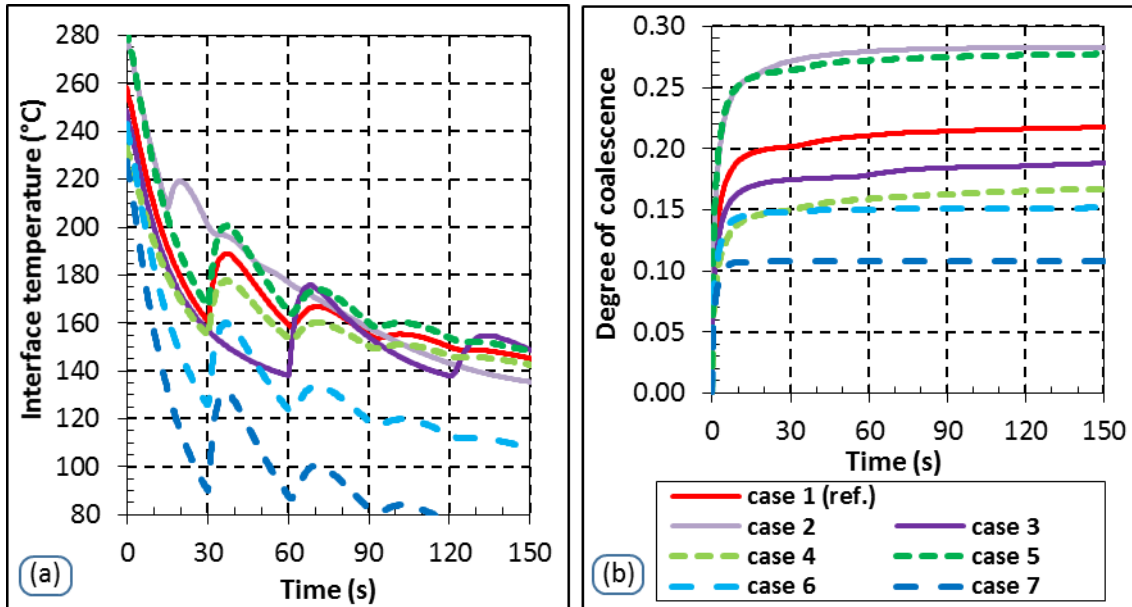


Figure 16 – (a) Thermal history of the interface between filaments for different configurations, and (b) the corresponding degree of coalescence evolution.

For cases 1, 2, and 3, the results in Figure 16 show that the degree of coalescence decreases from $D_{\text{coalescence}} = 0.28$ to 0.19 when the time between two depositions increases from 15 s to 60 s. This happens when the extruded filament does not cool to ambient temperature between depositions. In this situation, the final user should accelerate the filament deposition to increase the final coalescence level.

For cases 1, 4, and 5, the extrusion temperature varies from 300 to 380°C. The temperature evolutions present a small offset between these three configurations. However, it induces greater differences on the degree of coalescence, varying from $D_{\text{coalescence}} = 0.17$ to 0.28. Thus, in the case where a maximum degree of coalescence is the objective, the final user should pick the highest temperature to facilitate the coalescence but should take care not to degrade the polymer. For example, degradation is observed in less than 60 min at 400°C for PEKK KEPSTAN™ 6002 grade [6].

For cases 1, 6 and 7, when the heating chamber temperature varies from cycles at 50–65°C to cycles at 130–145°C, it triggers an increase from $D_{\text{coalescence}} = 0.11$ to 0.22. This shows the final user the importance of using a high temperature chamber to obtain a good final degree of coalescence.

5. Conclusion

This work developed a method to assess the quality of the adhesion between two filaments in the FFF process, from knowledge of the thermal history at the interface and from the thermophysical properties of the material. We presented this methodology, with (i) an experimental study on heat transfer of the FFF process for the high performance PEKK polymer, (ii) characterization of the thermal properties of the polymer, (iii) development of a

simulation model to predict the temperature at the interface of the filaments, (iv) characterization of the three properties linked to the adhesion, and (v) post-processing of the thermal history at the interface to model the evolution of the adhesion reached through coalescence and interface healing processes.

The main contributions of this work are the following. First, in terms of heat transfer, the development of an instrumented bench, including a high temperature chamber and plate able to print high performance polymers such as PEKK, enabled temperature measurement at the filament scale with an infrared camera on a wall geometry. The conditions of measurement were validated when the measurement was performed above a threshold layer to avoid reflections inside the heating chamber. Then, a 2D transient heat transfer model was developed and validated with the experimental results. This model was used to show the influence of the heating plate up to the 8th deposited filament. Finally, these numerical and experimental tools provide a better understanding of heat transfer and adhesion in the FFF process. Thermal heterogeneity was quantified between the core, surface, and interface of the filaments and heat transfer modes were analyzed, showing that 57% of the cooling was by conduction with the previous filaments and 43% by convective and radiative effects.

The main contribution on adhesion was the use of both coalescence and interface healing models. From the knowledge gained about surface tension, viscosity, and relaxation time in isothermal conditions, we propose a new tool to help the final user get an idea of the two kinetic processes: TTC and TTH diagrams. Finally, our parametric study provides guidelines for the final user, about the time between two depositions, the extrusion temperature and the heating chamber temperature.

The major novelties in the present work are the following. First, we focused on the filament scale, where several other studies are at the part scale. Then, experimental setup is fully controlled in terms of temperatures, boundary conditions and calibrated measurement techniques under high temperature (required with the PEKK deposition). Finally, the numerical simulation shows the importance of the thermal gradients at the filament scale and their effect on the adhesion and coalescence.

The presented framework was applied to a simplified geometry, a single filament wall. In the case of more realistic three-dimensional geometries, the two-dimensional cross section approximation can still be applied. The coupled thermal and adhesion physics presented above would remain similar. Implementation would then be extended and account for the neighboring filaments contact. Nonetheless, such developments would increase number of deposition steps, complexify the geometries and extend the numerical resolution times.

In this work, the analytical coalescence model is based on strong assumptions (free coalescence, Newtonian behavior, ideal geometries). In a future work, a model with a better fidelity may be developed to gain a more reliable understanding of the interlayer adhesion. This may include coupled bonding effects [4, 61]. It will also be correlated to the mechanical interlayer adhesion quality measured thanks to an adequate experimental setup.

6. Acknowledgments

This study is part of the FACT project managed by IRT Jules Verne (French Institute of Research and Technology in Advanced Manufacturing Technologies for Composite, Metallic, and Hybrid Structures). The authors wish to acknowledge the industrial and academic partners of this project: AIRBUS, ARKEMA, DAHER,

DEDIENNE, EOS, LIEBHERR, SAFRAN, ZODIAC ENGINEERING, CANOE, TOBECA, LTEN, PIMM, CNRS, ENSAM, and the University of Nantes. This project is partly funded by the grant ANR-10-AIRT-02.

The authors also want to thank staff from LTeN: Gwenaël Biotteau and Nicolas Lefevre, for their help with the design and fabrication of the experimental bench. We also thank Violaine Le Louet from Capacités S.A.S, the Engineering and Research valuation subsidiary of Nantes University for her help with the rheological characterization of the polymer relaxation time.

7. References

- [1] A. 52900:2015, Standard Terminology for Additive Manufacturing – General Principles – Terminology, ASTM Int. i (2015) 1–9.
http://compass.astm.org/EDIT/html_annot.cgi?ISOASTM52900+15.
- [2] T.T. Wohlers, I. Campbell, O. Diegel, R. Huff, J. Kowen, Wohlers Report 2019, 2019.
- [3] M. Jani, Ultimaker report - Comparing FFF, SLA, and SLS technologies, (2018).
<https://ultimaker.com/learn/comparing-fff-sla-and-sls-technologies>.
- [4] R.P. Wool, K.M. O'Connor, A theory of crack healing in polymers, *J. Appl. Phys.* 52 (1981) 5953–5963. <https://doi.org/10.1063/1.328526>.
- [5] ARKEMA, R. REBER, PEKK 3D Printing Brochure - A basic overview of Kepstan® PEKK performance versus traditional PEEK resins, 2018.
- [6] T. Choupin, Mechanical performances of PEKK thermoplastic composites linked to their processing parameters, Thesis, Paris Institute of Technology, ENSAM, 2017.
- [7] M.A. Yardimci, S. Danforth, A phenomenological numerical model for fused deposition processing of particle filled parts, *Solid Free. Fabr. Symp.* (1995) 189–195.
<http://utwired.engr.utexas.edu/lff/symposium/proceedingsArchive/pubs/Manuscripts/1995/1995-23-Yardimci.pdf>.
- [8] M.A. Yardimci, S. Güçeri, Conceptual framework for the thermal process modelling of fused deposition, *Rapid Prototyp. J.* 2 (1996) 26–31. <https://doi.org/10.1108/13552549610128206>.
- [9] L. Li, Q. Sun, C. Bellehumeur, P. Gu, Investigation of bond formation in FDM process, *Solid Free. Fabr. Proc.* (2002) 400–407. <https://doi.org/10.1108/13552540810862028>.
- [10] C. Bellehumeur, L. Li, Modeling of Bond Formation Between Polymer Filaments in the Fused Deposition Modeling Process, *J. Manuf. Process.* 6 (2004) 170–178.
[https://doi.org/10.1016/S1526-6125\(04\)70071-7](https://doi.org/10.1016/S1526-6125(04)70071-7).
- [11] J.P. Thomas, J.F. Rodriguez, Modeling the Fracture Strength Between Fused-Deposition Extruded Roads, *Solid Free. Fabr. Proc.* (2000) 17–23.
- [12] Q. Sun, G.M. Rizvi, C.T. Bellehumeur, P. Gu, Effect of processing conditions on the bonding quality of FDM polymer filaments, *Rapid Prototyp. J.* 14 (2008) 72–80.
<https://doi.org/10.1108/13552540810862028>.
- [13] S.F. Costa, F.M. Duarte, J.A. Covas, Thermal conditions affecting heat transfer in FDM/FFE: a contribution towards the numerical modelling of the process, *Virtual Phys. Prototyp.* 10 (2014) 35–46. <https://doi.org/10.1080/17452759.2014.984042>.
- [14] S.F. Costa, Free Form Extrusion: Extrusion of 3D Components Using Complex Polymeric Systems, University of Minho, 2012.
http://www3.dsi.uminho.pt/seeum2010/CD/abstracts/1708_4.pdf.
- [15] C. Ionescu, S. Costa, F. Duarte, J.A. Covas, Matlab, an ubiquitous tool for the practical engineer - Using matlab to compute heat transfer In free form extrusion, 2011.
<https://biblio.ugent.be/publication/1955415/file/1956703.pdf#page=465>.
- [16] J. Zhang, X.Z. Wang, W.W. Yu, Y.H. Deng, Numerical investigation of the influence of process conditions on the temperature variation in fused deposition modeling, *Mater. Des.* 130

- (2017) 59–68. <https://doi.org/10.1016/j.matdes.2017.05.040>.
- [17] B. Brenken, E. Barocio, A. Favaloro, V. Kunc, R.B. Pipes, Development and validation of extrusion deposition additive manufacturing process simulations, *Addit. Manuf.* 25 (2019) 218–226. <https://doi.org/10.1016/j.addma.2018.10.041>.
- [18] A.J. Favaloro, B. Brenken, E. Barocio, R.B. Pipes, Simulation of Polymeric Composites Additive Manufacturing using Abaqus, *Sci. Age Exp.* (2017) 103–114. <https://www.3ds.com/fileadmin/PRODUCTS/SIMULIA/PDF/scc-papers/2017/simulation-polymeric-composites-am-purdue-favaloro.pdf>.
- [19] D. Xu, Y. Zhang, F. Pigeonneau, Thermal analysis of the fused filament fabrication printing process: Experimental and numerical investigations, *Int. J. Mater. Form.* (2020). <https://doi.org/10.1007/s12289-020-01591-8>.
- [20] C. Kousiatza, D. Karalekas, In-situ monitoring of strain and temperature distributions during fused deposition modeling process, *Mater. Des.* 97 (2016) 400–406. <https://doi.org/10.1016/j.matdes.2016.02.099>.
- [21] F. Peng, B.D. Vogt, M. Cakmak, Complex flow and temperature history during melt extrusion in material extrusion additive manufacturing, *Addit. Manuf.* 22 (2018) 197–206. <https://doi.org/10.1016/j.addma.2018.05.015>.
- [22] S.F. Costa, F.M. Duarte, J.A. Covas, Estimation of filament temperature and adhesion development in fused deposition techniques, *J. Mater. Process. Technol.* 245 (2017) 167–179. <https://doi.org/10.1016/j.jmatprotec.2017.02.026>.
- [23] R.B. Dinwiddie, L.J. Love, J.C. Rowe, Real-time process monitoring and temperature mapping of a 3D polymer printing process, *Proc. SPIE - Int. Soc. Opt. Eng.* (2013). <https://doi.org/10.1117/12.1518454>.
- [24] J.E. Seppala, K.D. Migler, Infrared thermography of welding zones produced by polymer extrusion additive manufacturing, *Addit. Manuf.* 12 (2016) 71–76. <https://doi.org/10.1016/j.addma.2016.06.007>.
- [25] J.E. Seppala, S. Hoon Han, K.E. Hillgartner, C.S. Davis, K.B. Migler, Weld formation during material extrusion additive manufacturing, *Soft Matter.* 13 (2017) 6761–6769. <https://doi.org/10.1039/c7sm00950j>.
- [26] E. Ferraris, J. Zhang, B. Van Hooreweder, Thermography based in-process monitoring of Fused Filament Fabrication of polymeric parts, *CIRP Ann.* 68 (2019) 213–216. <https://doi.org/10.1016/j.cirp.2019.04.123>.
- [27] J. Frenkel, Viscous Flow of Crystalline Bodies under the Action of Surface Tension, *J. Phys.* 9 (1945) 385. <http://ci.nii.ac.jp/naid/10008662610/en/> (accessed June 6, 2018).
- [28] J. Eshelby, Discussion of ‘Seminar on the Kinetics of Sintering,’ *Metall. Trans.* 185 (1949) 796–813.
- [29] O. Pokluda, C.T. Bellehumeur, J. Machopoulos, Modification of Frenkel’s Model for Sintering, *AIChE J.* 43 (1997) 3253–3256. <https://doi.org/10.1002/aic.690431213>.
- [30] D.O. Kazmer, T.J. Coogan, J. Mead, C. Barry, S. Johnston, R. Malloy, M. Sobkowicz-Kline, J. Vangness, P. Casey, D. Rondeau, A. Moshe, A Protocol for Filament Production and Use in Fused Deposition Modeling, *Spe Antec.* (2016) 881–886.
- [31] M. Faes, E. Ferraris, D. Moens, Influence of Inter-layer Cooling time on the Quasi-static Properties of ABS Components Produced via Fused Deposition Modelling, *Procedia CIRP.* 42 (2016) 748–753. <https://doi.org/10.1016/j.procir.2016.02.313>.
- [32] L. Li, Q. Sun, C. Bellehumeur, P. Gu, Composite Modeling and Analysis for Fabrication of FDM Prototypes with Locally Controlled Properties, *J. Manuf. Process.* 4 (2002) 129–141. [https://doi.org/10.1016/S1526-6125\(02\)70139-4](https://doi.org/10.1016/S1526-6125(02)70139-4).
- [33] S. Bakrani Balani, C. France, N. Valerie, Toward improvement of the properties of parts manufactured by FFF (fused filament fabrication) through understanding the influence of temperature and rheological behaviour on the coalescence phenomenon, in: *AIP Conf. Proc.* 1896, 2017.

- [34] R.W. Hopper, Coalescence of Two Viscous Cylinders by Capillarity: Part I, Theory, *Am. Ceram. Soc.* 76 (1993) 2947–52.
- [35] R.W. Hopper, Coalescence of Two Viscous Cylinders by Capillarity: Part II, Shape Evolution, *Am. Ceram. Soc.* 76 (1993) 2953–2960.
- [36] S. Bakrani Balani, C. Arthur, C. France, N. Valérie, Influence of parameters controlling the extrusion step in fused filament fabrication (FFF) process applied to polymers using numerical simulation, *AIP Conf. Proc.* 1960 (2018). <https://doi.org/10.1063/1.5034995>.
- [37] P.G. de Gennes, Reptation of a Polymer Chain in the Presence of Fixed Obstacles, *J. Chem. Phys.* 55 (1971) 572–579. <https://doi.org/10.1063/1.1675789>.
- [38] ARKEMA, KEPSTAN PEKK Brochure - A basic overview of grades and performance properties, 2018. <https://www.extremematerials-arkema.com/en/product-families/kepstan-pekk-polymer-range/>.
- [39] T. Choupin, B. Fayolle, G. Régnier, C. Paris, J. Cinquin, B. Brulé, Isothermal crystallization kinetic modeling of poly(etherketoneketone) (PEKK) copolymer, *Polymer (Guildf)*. 111 (2017) 73–82. <https://doi.org/10.1016/j.polymer.2017.01.033>.
- [40] B. Pignon, X. Tardif, N. Lefèvre, V. Sobotka, N. Boyard, D. Delaunay, A new PvT device for high performance thermoplastics: Heat transfer analysis and crystallization kinetics identification, *Polym. Test.* 45 (2015) 152–160. <https://doi.org/10.1016/j.polymertesting.2015.05.013>.
- [41] P. Tait, *Physics and Chemistry of the voyage of H.M.S Challenger*, Londres. 2 (1888).
- [42] G. Tammann, Über die Abhängigkeit der Volumina von Lösungen vom Druck, *Z. Phys. Chemi.* 17 (1895) 620.
- [43] J.H. Dymond, R. Malhotra, The Tait equation: 100 years on, *Int. J. Thermophys.* 9 (1988) 941–951. <https://doi.org/10.1007/BF01133262>.
- [44] B. Pignon, *Cristallisation des polymères semi-cristallins en condition thermique extrême*, University of Nantes, LTEN, 2015.
- [45] A. Lepoivre, A. Levy, N. Boyard, V. Gaudefroy, V. Sobotka, Coalescence in fused filament fabrication process: thermo-dependent characterization of high-performance polymer properties, *Polym. Test.* [under rev (2021)].
- [46] FLIR, FLIR SC7000 MWIR Series - IR camera datasheet, 2014.
- [47] FLIR, FLIR SC7000 - MW 50mm F/2.0 Lens - IR camera objective datasheet, n.d.
- [48] A. Lepoivre, N. Boyard, A. Levy, V. Sobotka, Heat Transfer and Adhesion Study for the FFF Additive Manufacturing Process, *Procedia Manuf.* 47 (2020) 948–955. <https://doi.org/10.1016/j.promfg.2020.04.291>.
- [49] A. Lepoivre, Étude des transferts thermiques et de l'adhésion à l'échelle du cordon dans le procédé de fabrication additive FFF (extrusion de filament fondu), Thesis, Nantes University, LTEN (UMR CNRS 6607), IRT Jules Verne, 2021.
- [50] K. Hirao, M. Tomozawa, Kinetics of Crack Tip Blunting of Glasses, *J. Am. Ceram. Soc.* 70 (1987) 43–48. <https://doi.org/10.1111/j.1151-2916.1987.tb04851.x>.
- [51] D. Defauchy, *Simulation du procédé de fabrication directe de pièces thermoplastiques par fusion laser de poudre*, Paris Institute of Technology, ENSAM, 2013.
- [52] S. Prager, M. Tirrell, The healing process at polymer-polymer interfaces, *J. Chem. Phys.* 75 (1981) 5194–5198. <https://doi.org/10.1063/1.441871>.
- [53] R.P. Wool, B.L. Yuan, O.J. McGarel, Welding of polymer interfaces, *Polym. Eng. Sci.* 29 (1989) 1340–1367. <https://doi.org/10.1002/pen.760291906>.
- [54] F. Yang, R. Pitchumani, Healing of thermoplastic polymers at an interface under nonisothermal conditions, *Macromolecules.* 35 (2002) 3213–3224. <https://doi.org/10.1021/ma010858o>.
- [55] J. Avenet, A. Levy, J.L. Bailleul, S. Le Corre, J. Delmas, Adhesion of high performance thermoplastic composites: Development of a bench and procedure for kinetics identification, *Compos. Part A Appl. Sci. Manuf.* 138 (2020).

- <https://doi.org/10.1016/j.compositesa.2020.106054>.
- [56] D. Delaunay, P. Le Bot, R. Fulchiron, J.F. Luye, G. Regnier, Nature of contact between polymer and mold in injection molding. Part I: influence of a non-perfect thermal contact, *Polym. Eng. Sci.* 40 (2000) 1682–1691. <https://doi.org/10.1002/pen.11300>.
- [57] A. Bendada, A. Derdouri, M. Lamontagne, Y. Simard, Analysis of thermal contact resistance between polymer and mold in injection molding, *Appl. Therm. Eng.* 24 (2004) 2029–2040. <https://doi.org/10.1016/j.applthermaleng.2003.12.027>.
- [58] R. Le Goff, G. Poutot, D. Delaunay, R. Fulchiron, E. Koscher, Study and modeling of heat transfer during the solidification of semi-crystalline polymers, *Int. J. Heat Mass Transf.* 48 (2005) 5417–5430. <https://doi.org/10.1016/j.ijheatmasstransfer.2005.06.015>.
- [59] J. Avenet, T. Cender, S. Le Corre, J-L. Bailleul, A. Levy, Experimental correlation of rheological relaxation and interface healing times in welding thermoplastic PEKK composites. *Composites - Part A: Applied Science and Manufacturing*, 149. (2021) <https://doi.org/10.1016/j.compositesa.2021.106489>
- [60] E. Barocio, B. Brenken, A.J. Favaloro, R.B. Pipes, Interlayer fusion bonding of semi-crystalline polymer composites in extrusion deposition additive manufacturing. *Composites Science and Technology*, in press (2022), <https://doi.org/10.1016/j.compscitech.2022.109334>
- [61] C. A. Butler, R. L. McCullough, R. Pitchumani, J. W. Gillespie, An analysis of mechanisms governing fusion bonding of thermoplastic composites. *Journal of Thermoplastic Composite Materials*, 11(4), 338 (1998),